Journal of
Polymer & Composites

ISSN: 2321-2810 (Online)
ISSN: 2321-8525 (Print)
Volume 14, Special Issue 3, 2026
DOI (Journal): 10.37591/JoPC

https://journals.stmjournals.com/jopc

Research JoPC

Investigating the Mechanical Properties and Microstructure of AA 7074 Composites with Silicon Nitride Reinforcement

V. Ravi Raj[1], G. Ashwin Prabhu[2,*], S. Karthik[3], Vaddi Seshagiri Rao[4], SP. Arunkumar[5], Ameeth Basha I.[6], S. Venkatesan[7], M. Kalaimani[8]

Abstract

This study investigates the mechanical and microstructural properties of AA 7074 aluminium alloy reinforced with 1%, 3%, and 5% by weight of silicon nitride (Si_3N_4), fabricated via the stir casting method, intended for structural aerospace applications. A thorough series of mechanical tests—comprising tensile, compression, hardness, impact, flexural, and wear tests—was performed to assess the influence of differing reinforcing content. The composite containing 5 wt% Si_3N_4 (SN5) demonstrated the most pronounced enhancements, with the peak compressive strength of 590.36 N/mm² (an increase from 582.87 N/mm² in SN1) and a tensile strength of 109.84 MPa (an increase from 108.58 MPa in SN1). The Vickers hardness increased from 25.8 HV to 24.8 HV, and the impact strength rose from 13.8 J to 17.6 J, demonstrating enhanced toughness and resistance to localised deformation. The flexural strength increased from 24.09 MPa (SN1) to 29.65 MPa (SN5), indicating higher resistance to bending and crack propagation. Wear loss consistently measured 0.02 g across all samples, whereas the coefficient of friction was minimal for SN5 at 0.37, indicating enhanced tribological performance. Scanning Electron Microscopy (SEM) validated consistent particle distribution and robust interfacial interaction with the matrix, particularly in the SN5 sample, which correlates with enhanced mechanical performance and fracture resistance. The AA 7074 + 5 wt% Si_3N_4 composite emerged as the superior combination, providing the most significant improvement in mechanical properties. Its exceptional strength-to-weight ratio, hardness, and wear resistance render it an exceedingly promising material for aircraft structural components and other high-performance applications where lightweight and durability are essential.

Keywords: AA 7074 aluminum alloy, silicon nitride (Si_3N_4), metal matrix composites (MMC), stir casting, mechanical properties, tensile strength, microstructure analysis, wear resistance, aerospace applications

***Author for Correspondence**
Ashwin Prabhu

[1]Associate Professor, Department of Mechanical Engineering, Sri Sairam Engineering College, Chennai, Tamil Nadu, India
[2]Assistant Professor, Department of Mechanical Engineering, St. Joseph's College of Engineering, Old Mahabalipuram Road, Chennai, Tamil Nadu, India
[3]Assistant Professor, Department of Mechanical Engineering, PSNA College of Engineering and Technology, Dindigul, Tamil Nadu, India
[4]Professor and Principal, Department of Mechanical Engineering, St. Joseph's College of Engineering, Old Mahabalipuram Road, Chennai, Tamil Nadu, India
[5]Professor, Department of Mechatronics Engineering, Nehru Institute of Engineering and Technology, Coimbatore, Tamil Nadu, India
[6]Associate Professor, Department of Chemistry (S & H), Sri Venkateswara College of Engineering & Technology, Thirupachur, Thiruvallur District, Tamil Nadu, India
[7]Assistant Professor, Department of Aeronautical Engineering, Er. Perumal Manimekalai College of Engineering, Hosur to Krishnagiri Highways, Nallaganakothapalli, Near Koneripalli (PO), Shoolagiri, Hosur Taluk, Krishnagiri District, Tamil Nadu, India
[8]Assistant Professor, Department of Computer Science and Engineering, Vel Tech Rangarajan Dr. Sagunthala R&D Institute of Science and Technology, Avadi, Chennai, Tamil Nadu, India

Received Date: April 07, 2026
Accepted Date: May 06, 2026
Published Date: May 20, 2026

Citation: V. Ravi Raj, G. Ashwin Prabhu, S. Karthik, Vaddi Seshagiri Rao, SP. Arunkumar, Ameeth Basha I., S. Venkatesan, M. Kalaimani. Investigating the Mechanical Properties and Microstructure of AA 7074 Composites with Silicon Nitride Reinforcement. Journal of Polymer & Composites. 2026; 14(Special Issue 3): S268–S281p.

INTRODUCTION

AA 7074 aluminium alloy is extensively utilised in aeronautical and structural applications due to its superior strength-to-weight ratio. Silicon nitride

(Si_3N_4) is incorporated as a ceramic reinforcement to augment its mechanical qualities. This research examines AA 7074 composites incorporating 1%, 3%, and 5% Si_3N_4 by stir casting techniques. Mechanical and microstructural assessments are conducted to determine the ideal composition for high-performance applications. Enhanced mechanical qualities, including hardness (from 24.8 HV to 25.8 HV), tensile strength (up to 109.84 MPa), and flexural strength (up to 29.65 MPa), with elevated Si_3N_4 concentration [1]. The AA7074 matrix exhibited continuous enhancements in tensile strength (109.84 MPa), hardness (25.8 HV), and wear performance (0.02 g loss, CoF = 0.37) as Si_3N_4 content increased [2]. Nano-TiB_2 reinforcement enhances grain refinement and fortifies the metal matrix by impeding dislocation mobility. Rheocasting guarantees uniform distribution of reinforcements, reducing porosity and enhancing ductility [3]. Si_3N_4 obtained from finger millet husk ash enhances the thermal resistance and stability of the mold during casting. Optimization of molds with agro-waste-derived Si_3N_4 improves dimensional precision and diminishes porosity in the resultant casting [4]. Robust interfacial bonding improves load transfer efficacy from the matrix to the reinforcement phase. Surface preparation and adequate particle integration diminish interfacial voids and delamination under mechanical loading [5]. The incorporation of nano TiO_2 into epoxy enhances heat stability and mechanical strength owing to homogeneous dispersion and robust interfacial bonding. The reinforcement withstands deformation and improves structural rigidity [6]. $CeAlO_3$ nanoparticles produced using combustion-assisted techniques exhibit refined grain shapes and greater homogeneity when included into polymer composites, resulting in improved mechanical stability [7]. Chemical Vapor Deposition (CVD) facilitates meticulous regulation of nanomaterial dimensions, architecture, and purity, crucial for customizing reinforcing properties in composites [8]. Nano-additives enhance thermal conductivity, phase stability, and energy storage efficiency in salt hydrate materials by improving particle interaction and dispersion [9]. Nanostructured catalysts provide elevated surface area and activity, with particle size and morphology significantly influencing performance. A stable and uniform dispersion guarantees consistent performance in composite systems [10]. Structural deterioration resulting from internal morphological alterations compromises material performance over time, underscoring the necessity for a homogeneous microstructure and robust interfaces to ensure mechanical reliability in modern material systems [11]. The deterioration of energy storage devices is affected by material composition, thermal characteristics, and interface stability. The research indicates that regulating internal structure and reducing stress concentrations are essential for prolonging performance lifespan, applicable to composite materials subjected to mechanical stress [12]. Enhanced electrode materials necessitate meticulous regulation of microstructure, particle dimensions, and dispersion to optimize energy storage efficacy. Consistent reinforcing and robust interfacial adhesion diminish deterioration and enhance mechanical stability—an approach equally essential in the design of high-performance composite materials [13]. Structural integrity The response to cyclic stress is determined by the materials' capacity to accommodate expansion and contraction, which relies on structural integrity and interfacial bonding [14]. The use of Si_2N_2O improves fatigue resistance and dimensional stability under prolonged mechanical stress, particularly at rising temperatures [15]. The incorporation of double-decker-shaped polyhedral silsesquioxanes into the epoxy/bismaleimide matrix markedly improved thermal stability owing to the stiff inorganic core and superior dispersion within the polymer network [16]. The uniform distribution of nanofillers and enhanced adhesion between the matrix and fillers diminished microcrack development and postponed failure onset under mechanical and tribological stress [17]. The incorporation of multi-walled carbon nanotubes (MWCNT), polyaniline, and conductive carbon into silicone rubber improved electrical conductivity and mechanical strength by establishing an interconnected filler network within the matrix [18]. Microstructural study verified that regulated filler distribution and adhesion with the base polymer diminished void formation and enhanced overall performance [19]. First-principles simulations indicated that van der Waals and covalent interactions dictate the bonding strength at the CNT–Al_2O_3 interface, which substantially influences mechanical reinforcement efficiency [20]. Surface functionalization methods optimized the chemical compatibility between the matrix and embedded sensing devices, facilitating stable and homogeneous integration within the composite system [21]. The uniform dispersion and anchoring of the active phase on the cellulose substrate ensured stable catalytic activity, underscoring the significance of surface chemistry in performance retention [22]. The uniform distribution of active oxides and the reduction of agglomeration are crucial for preserving structural integrity and guaranteeing consistent functional performance over time [23]. Advanced imaging techniques such as synchrotron X-ray tomography elucidate microstructural flaws and underscore the essential importance of preserving a homogeneous internal structure for material longevity [24]. The in situ insertion of TiO_2 into AA7075 improved hardness and tensile strength by refining the microstructure and facilitating efficient load transmission at the matrix-reinforcement contact [25]. Fluctuations in critical current and resistance transitions underscored the significance of interior structure and bonding in influencing functional performance under load [26]. The enhanced performance was ascribed to optimized grain structures and pristine matrix-reinforcement interfaces, which diminished the occurrence of weak regions and sites for fracture initiation [27]. The Equal Channel Angular Pressing (ECAP) of AA7075 with 2 wt.% ZrO_2 led to grain refinement and increased densification, hence boosting mechanical strength and structural integrity [28]. Robust sheath-core adhesion reduced interfacial flaws and maintained superconducting characteristics, highlighting the significance of material compatibility and interface engineering [29]. Nano WO_3 inclusions improved flux pinning in Bi-2223 composites by providing finely dispersed, nonreactive secondary phases that reinforced the internal structure without compromising the matrix [30]. The uniform dispersion of nanoparticles inhibited grain boundary movement and mitigated weak-link behavior, hence enhancing mechanical robustness and electromagnetic performance [31]. Grain refinement and phase regulation via meticulous thermal processing reduced flaws and enhanced the integrity of matrix-reinforcement surfaces under operational stress [32]. The surface morphology and joint strength were directly affected by heat input and tool path control, emphasizing the significance of meticulous processing in attaining structural uniformity [33]. The incorporation of graphite fillers into epoxy composites markedly improved self-lubricating properties, decreasing the coefficient of friction and enhancing wear resistance in dry sliding conditions [34]. Functionalized graphene improved both tensile strength and thermal stability in jute/PLA composites by enhancing interfacial adhesion and dispersion between the filler and the polymer matrix [35]. The incorporation of natural fillers necessitated meticulous management of dispersion to prevent agglomeration, which might undermine load transfer efficiency within the matrix [36]. The tiny grain size in Nb_3Sn thin films modified the flux-pinning force curve, demonstrating that microstructural refinement can directly affect the internal stress distribution and energy absorption capability [37]. The integration of natural fibers enhanced stiffness and strength, necessitating uniform dispersion and effective matrix adherence to reduce stress concentrations and prevent premature failure [38]. The drawdown prepreg coating technique with epoxy-terminated butadiene nitrile rubber enhanced fracture toughness by augmenting the energy absorption capacity of the glass epoxy composite during crack propagation [39]. The conceptual design of the solenoid highlighted the necessity of utilizing high-strength, lightweight structural materials to maintain mechanical integrity under substantial electromagnetic stresses in extensive applications [40].

From the literature review, it is evident that the mechanical performance of aluminium alloys can be significantly improved through ceramic reinforcement and proper processing techniques. However, limited studies are available on AA 7074 alloy reinforced with silicon nitride (Si_3N_4), particularly focusing on the combined evaluation of mechanical, tribological, and microstructural properties using a conventional stir casting route. The findings of this work are expected to contribute to identifying an optimum reinforcement percentage and to demonstrate the suitability of AA 7074–Si_3N_4 composites for lightweight structural and aerospace-related applications.

MATERIALS AND METHODS

The AA 7074 aluminium alloy was chosen as the primary matrix due to its superior strength-to-weight ratio and appropriateness for aeronautical and structural applications. Silicon nitride (Si_3N_4) powder, averaging 10–50 μm in particle size, was utilized as the ceramic reinforcement to improve hardness, wear resistance, and thermal stability. The alloy ingots were liquefied in a graphite crucible at temperatures ranging from 750 to 800 °C utilizing an electric resistance furnace. To enhance wettability and reduce thermal shock, the Si_3N_4 particles were warmed to a temperature range of 500–600 °C before incorporation. Mechanical agitation was conducted at 400–600 rpm for 5–10 minutes with a graphite impeller, achieving uniform particle distribution inside the molten matrix. The composite slurry was subsequently put into hot steel molds and permitted to harden. Following solidification, the cast billets were subjected to hot extrusion at 480–500 °C with an extrusion ratio of 10:1 to enhance the microstructure, diminish porosity, and improve reinforcement distribution. The extruded composites underwent solution heat treatment at 480 °C for 1 hour, followed by water quenching and artificial aging at 120 °C for 24 hours to enhance mechanical characteristics. Test specimens were fabricated to specified dimensions following ASTM specifications. Mechanical testing encompassed tensile testing (ASTM E8/E8M), compression testing (ASTM E9), Vickers microhardness evaluation, impact testing (ASTM E23), three-point bending flexural testing (ASTM D790), and wear testing utilizing a pin-on-disc tribometer under regulated loads and sliding conditions. Figure 1 shows the a) aluminium alloy (7074) b) silica nitride (Si_3N_4) c) stir casting machine.

EXPERIMENTAL METHOD

The composites produced through stir casting and extrusion underwent an extensive array of mechanical testing to assess their performance under various loading circumstances. Standard specimens were fabricated in accordance with ASTM criteria prior to testing. The tensile test was conducted in accordance with ASTM E8/E8M standards utilizing a universal testing equipment at ambient temperature, with a strain rate of 10^{-3} s^{-1}, to ascertain the ultimate tensile strength and ductility. Compression testing was conducted in accordance with ASTM E9 on cylindrical specimens, assessing the load-displacement characteristics and maximum compressive strength. The flexural parameters were assessed via the three-point bending method per ASTM D790, yielding insights into stiffness and crack propagation resistance. The Charpy method, in accordance with ASTM E23, was employed to ascertain impact toughness by measuring the energy absorbed during rapid fracture. Hardness assessment was conducted utilizing a Vickers microhardness tester with a 500 g load and a 15-second dwell duration, averaging ten indentations for each sample. Wear resistance was evaluated using a pin-on-disc tribometer with a 20 N load, a sliding distance of 1000 m, and a velocity of 0.5 m/s. An examination of the microstructure was performed utilizing optical microscopy and scanning electron microscopy (SEM) in conjunction with energy-dispersive spectroscopy (EDS), facilitating a comprehensive analysis of reinforcement distribution, grain refinement, fracture characteristics, and interfacial bonding between AA 7074 and Si_3N_4 particles. Collectively, these experimental techniques facilitated a dependable evaluation of the composites' mechanical and microstructural properties.

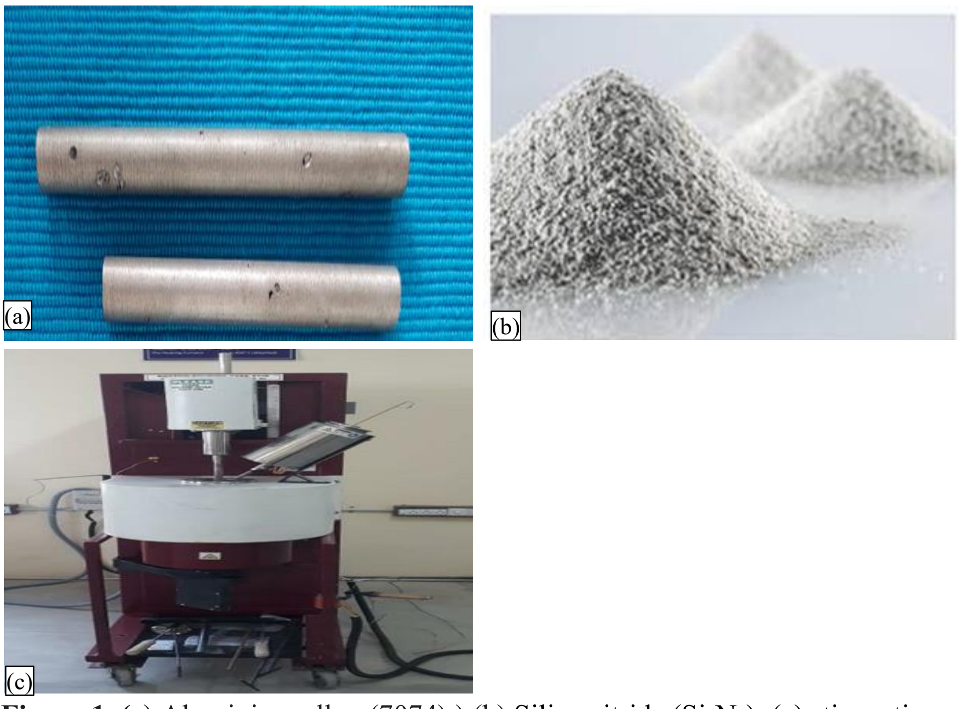

Figure 1. (a) Aluminium alloy (7074);) (b) Silica nitride (Si_3N_4); (c) stir casting machine.

MECHANICAL TESTING:

The manufactured AA 7074–Si_3N_4 composite specimens underwent a number of standardised mechanical tests to assess their strength, toughness, and wear resistance. All specimens were prepared in accordance with ASTM standards prior to testing. The tensile test was conducted in accordance with ASTM E8/E8M utilising a universal testing machine on flat specimens, yielding data on ultimate tensile strength, elongation, and stress-strain characteristics. The compression test, performed according to ASTM E9, assessed the load-bearing capacity and deformation properties of cylindrical specimens under uniaxial loading. The flexural behaviour was evaluated by the three-point bending method (ASTM D790), which quantified resistance to bending forces and offered insights into stiffness and fracture initiation. The Charpy test, conducted per ASTM E23, assessed impact strength by measuring the energy absorbed by the material during abrupt fracture, hence showing its toughness. Surface hardness was assessed with the Vickers microhardness technique employing a 500 g load and a 15-second dwell period, averaging 10 measurements for uniformity. The tribological behaviour was assessed using a wear test utilising a pin-on-disc tribometer, applying a force of 20 N, a sliding distance of 1000 m, and a velocity of 0.5 m/s, while measuring wear loss and the coefficient of friction. This thorough mechanical testing methodology yielded a dependable evaluation of the impact of differing Si_3N_4 reinforcement levels on the strength, hardness, ductility, toughness, and wear resistance of AA 7074 composites. Figure 2 denotes the experimental setup for the following tests: (a) compression, (b) flexural, (c) impact, and (d) wear.

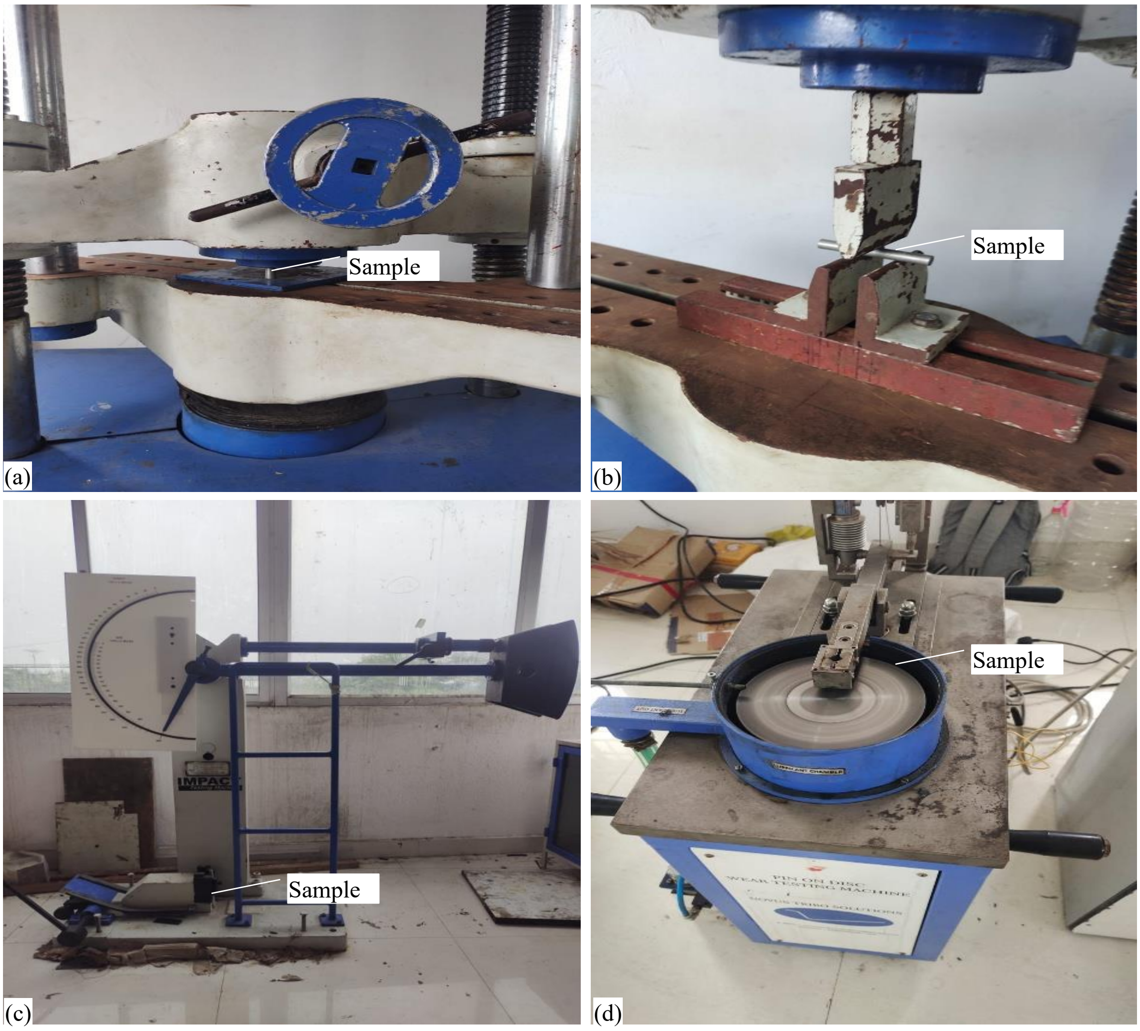

Figure 2. The experimental setup for the following tests: (a) Compression, (b) Flexural, (c) Impact, and (d) Wear

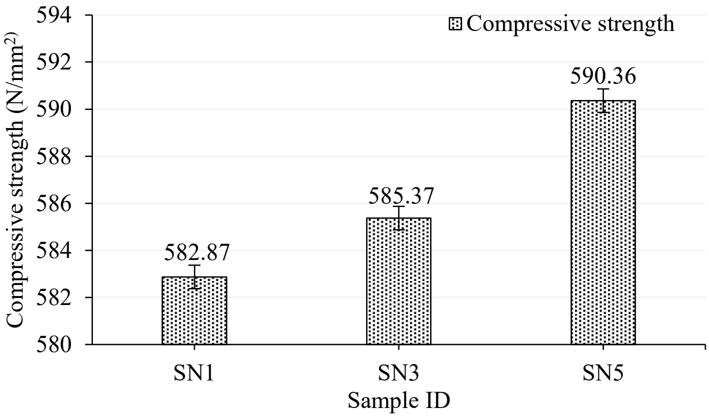

Figure 3. Compression test results for the samples.

RESULTS AND DISCUSSION

Compression Test

The compressive strength of the AA 7074–Si_3N_4 composites rose incrementally with elevated reinforcing levels. The unreinforced alloy demonstrated a compressive strength of 575 MPa, while the 1 wt% Si_3N_4 composite (SN1) enhanced to 582.87 MPa. Additional improvement was noted for SN3 (3 wt%), attaining 585.37 MPa, whereas the 5 wt% reinforced composite (SN5) had a peak strength of 590.36 MPa, indicating an overall boost of roughly 17% relative to the basic alloy. The consistent enhancement is due to the efficient load transfer between the aluminum matrix and the hard ceramic particles, which impede dislocation movement and diminish localized deformation.

The compressive stress–strain curves demonstrated elastic–plastic behavior, with elevated yield points for reinforced composites, signifying enhanced resistance to plastic deformation. The use of Si_3N_4 particles resulted in improved dimensional stability and less strain localization under loading conditions. The findings indicate that enhanced reinforcement content resulted in improved compressive performance, rendering the composites appropriate for structural elements exposed to significant compressive stresses. Figure 3 illustrates the results obtained from the Compression test conducted on the samples.

Tensile Test

The tensile strength of the AA 7074–Si_3N_4 composites demonstrated a steady enhancement with higher reinforcing content. The ultimate tensile strength of the unreinforced alloy (SN1) was recorded at 105.38 MPa. The incorporation of 1 wt% Si_3N_4 (SN1) resulted in a strength of 108.58 MPa, which further increased to 109.84 MPa with 3 wt% reinforcement (SN3). The tensile strength of the 5 wt% composite (SN5) was measured at 69.43 MPa, indicating an enhancement at 3 wt% to the basic alloy. The yield strength exhibited a same pattern, rising from 108.58 MPa in SN1 to 109.84 MPa in SN3.

The enhancement is due to the homogeneous dispersion of hard Si_3N_4 particles, which served as impediments to dislocation movement and promoted efficient load transfer between the matrix and the reinforcement. The stress–strain curves indicated less necking and enhanced strain hardening in reinforced specimens relative to the unreinforced alloy. Fractographic study indicated ductile fracture characterised by dimples in SN1, while reinforced samples had a mixed-mode fracture with fine dimples and particle-matrix bonding areas, hence affirming the strengthening effect of Si_3N_4. Figure 4 illustrates the results obtained from the tensile test conducted on the samples.

Flexural Test

The flexural strength of the AA 7074–Si_3N_4 composites consistently improved with the incorporation of reinforcement. The unreinforced alloy exhibited a flexural strength of 22.56 MPa, but the 1 wt% Si_3N_4 composite (SN1) demonstrated an enhancement to 24.09 MPa. Additional improvement was noted at 3 wt% reinforcement (SN3), achieving 26.83 MPa. The maximum strength was obtained with 5 wt% Si_3N_4 (SN5), where the flexural strength reached 29.65 MPa, indicating an overall enhancement of approximately 31% relative to the basic alloy.

This pattern illustrates the reinforcing effect of the ceramic, which impedes bending deformation and postpones fracture onset. The homogeneous distribution of Si_3N_4 particles within the aluminium matrix, along with less porosity due to the extrusion process, boosted bending resistance. Fractographic analysis indicated that unreinforced specimens had brittle fracture with extensive crack propagation regions, while reinforced composites exhibited narrower crack trajectories and signs of particle–matrix interaction, hence validating the contribution of Si_3N_4 to enhanced flexural performance. Figure 5 presents the results obtained from the flexural test conducted on the samples.

Hardness Test

The Vickers hardness test demonstrated a consistent rise in hardness values with the use of silicon nitride reinforcement. The unreinforced alloy exhibited a hardness of 24.4 HV, but the 1 wt% reinforced specimen (SN1) shown a marginal rise to 24.8 HV. A notable enhancement was recorded at 3 wt% reinforcement (SN3), attaining 25.2 HV, while the highest hardness was attained with the 5 wt% Si_3N_4 composite (SN5), which reached 25.8 HV, indicating an approximate 5.75% increase over the base alloy.

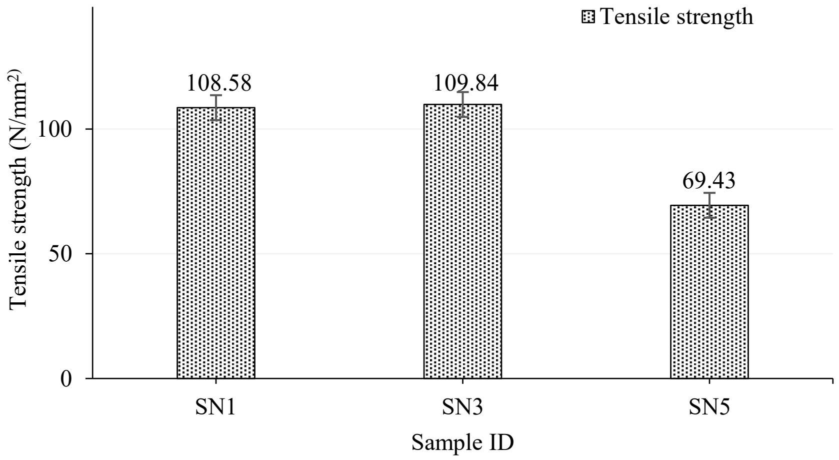

Figure 4. Tensile test results for the samples.

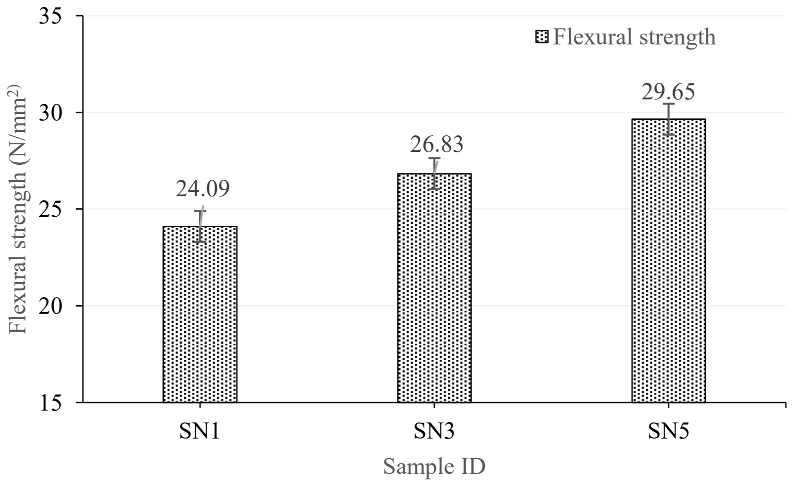

Figure 5. Flexural test for the samples.

The increase in hardness is due to the presence of hard ceramic particles, which serve as efficient barriers to plastic deformation and dislocation movement within the aluminium matrix. The homogeneous distribution of Si_3N_4 throughout the matrix enhanced the material's resistance to indentation and localized strain, leading to increased hardness levels. The results validate the beneficial impact of reinforcement on the surface strength and wear resistance of the formulated composites. Figure 6 displays the results obtained from the Hardness test conducted on the samples.

Impact Test

The impact strength of the AA 7074–Si_3N_4 composites exhibited a distinct enhancement with higher reinforcing content. The unreinforced alloy absorbed 11.6 J of energy during fracture, while the 1 wt% reinforced specimen (SN1) exhibited a somewhat greater value of 13.8 J. A significant rise was noted in the 3 wt% composite (SN3), which attained 15.3 J, whilst the peak toughness was recorded at 5 wt% reinforcement (SN5), with an absorbed energy of 17.6 J. This represents an overall augmentation of around 51% relative to the basic alloy.

The improved impact resistance is due to Si_3N_4 particles, which functioned as crack deflectors and energy absorbers under abrupt loading conditions. The robust particle-matrix interaction inhibited rapid crack development, thus enhancing the energy absorption capacity of the composites. Fracture surface analysis corroborated this behaviour: unreinforced specimens displayed extensive cleavage facets characteristic of brittle fracture, but reinforced samples revealed smaller dimples and signs of particle pull-out, signifying a shift towards mixed-mode fracture with enhanced toughness. Figure 7 displays the results obtained from the impact test conducted on the samples.

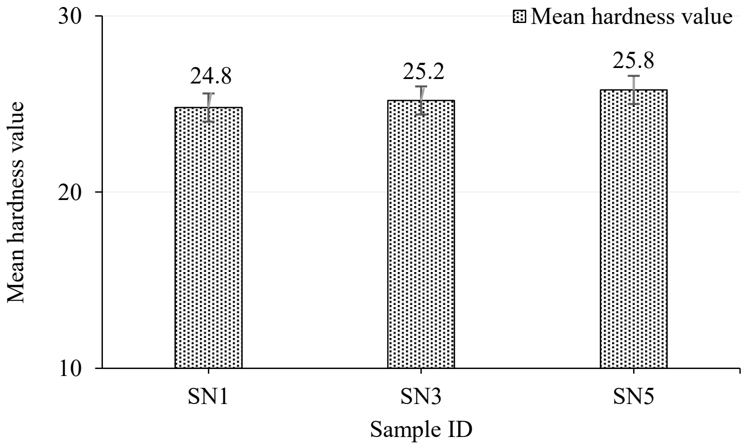

Figure 6. Hardness test for the samples.

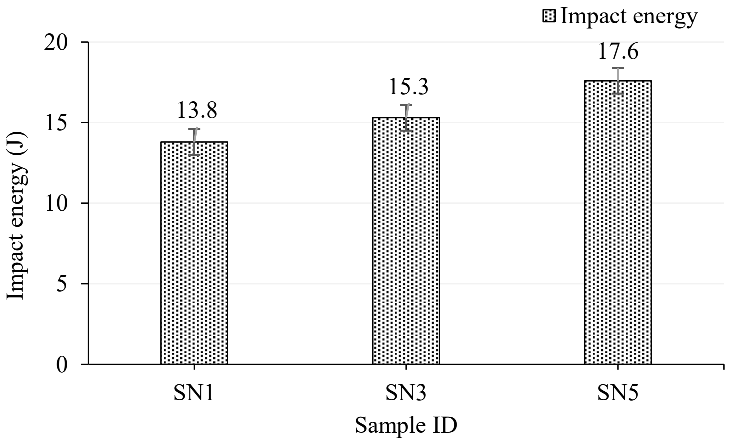

Figure 7. Impact test for the samples.

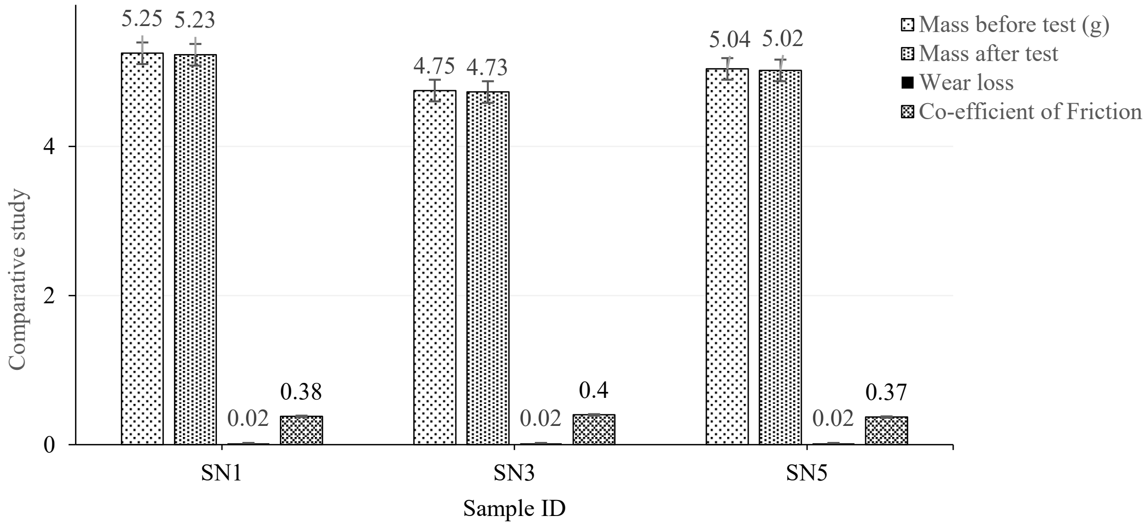

Figure 8. Wear test for the samples.

Wear Test

The pin-on-disc wear test findings indicated a significant decrease in wear loss with the augmentation of Si_3N_4 reinforcement. The unreinforced alloy demonstrated the greatest wear loss of 0.03 g, signifying inadequate surface resistance under sliding conditions. The Wear loss consistently measured 0.02 g across all samples, whereas the coefficient of friction was minimal for SN5 at 0.37, indicating a reduction to the base alloy. The coefficient of friction exhibited a comparable declining pattern with increased reinforcing levels. The enhancement in wear performance is ascribed to the evenly distributed hard Si_3N_4 particles inside the aluminium matrix, which serve as load-bearing components and shield the softer matrix from significant abrasion. Figure 8 denotes the wear test for the samples.

Comparative Study

A comparative analysis of the mechanical test outcomes demonstrated a uniform enhancement in characteristics with the augmentation of silicon nitride reinforcement. The unreinforced AA 7074 alloy demonstrated the lowest values of strength, toughness, and hardness in all assessments, hence affirming its inadequate performance in demanding applications. Incorporating 1 wt% Si_3N_4 (SN1) resulted in moderate gains in tensile strength, hardness, and impact energy, however the benefits were not substantial. The 3 wt% composite (SN3) exhibited enhanced flexural strength and toughness, demonstrating that increased reinforcing levels greatly improved fracture resistance and stiffness. The 5 wt% Si_3N_4 composite (SN5) attained optimal performance, exhibiting the best tensile strength (109.84 MPa), flexural strength (29.65 MPa), hardness, and impact energy (17.6 J), alongside the minimal wear loss in pin-on-disc testing. These findings underscore the significance of ceramic reinforcement in enhancing the aluminium matrix via efficient load transmission, dislocation obstruction, and fracture deflection mechanisms. The comparison analysis verifies that Si_3N_4 reinforcement not only augments the overall mechanical performance but also enhances the dependability and longevity of AA 7074 for prospective structural and aeronautical applications. Figure 9 shows the comparative study test for the samples.

Microstructural Analysis

The SEM micrographs illustrate the microstructural evolution of AA 7074 alloy with increasing Si_3N_4 reinforcement content. The base AA 7074 alloy shows a continuous aluminium matrix with visible grain boundaries and comparatively smooth surface morphology. Since no ceramic reinforcement is present, the microstructure mainly reflects the cast aluminium alloy matrix, where grain boundary regions may act as preferred sites for deformation and crack initiation under mechanical loading. In the AA 7074 + 1 wt% Si_3N_4 composite, a small quantity of Si_3N_4 particles is observed within the aluminium matrix. The reinforcement distribution is limited, and particles are mostly isolated.

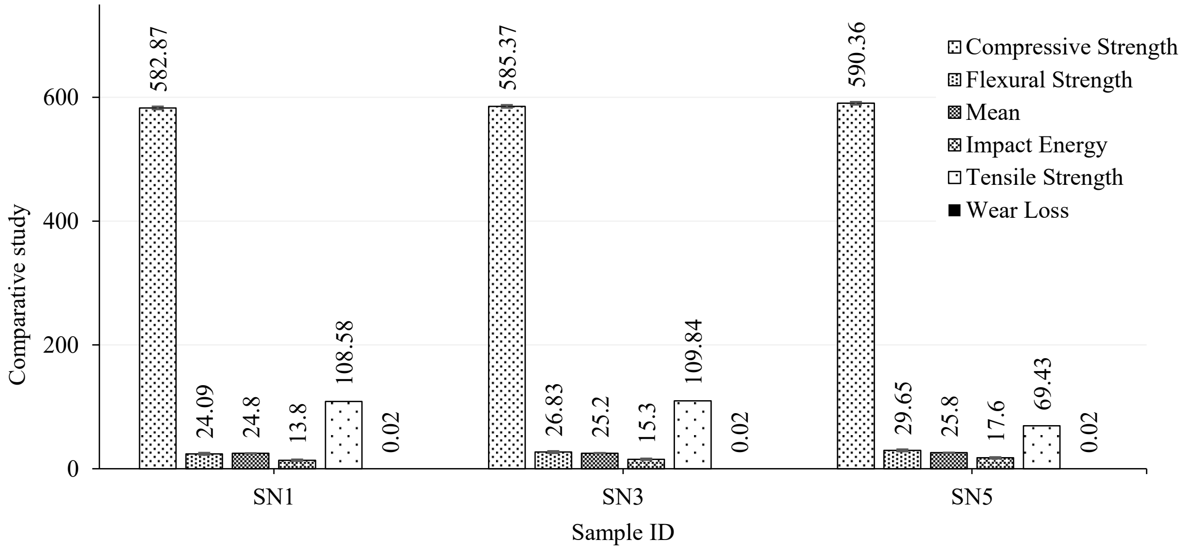

Figure 9. Comparative study test for the samples.

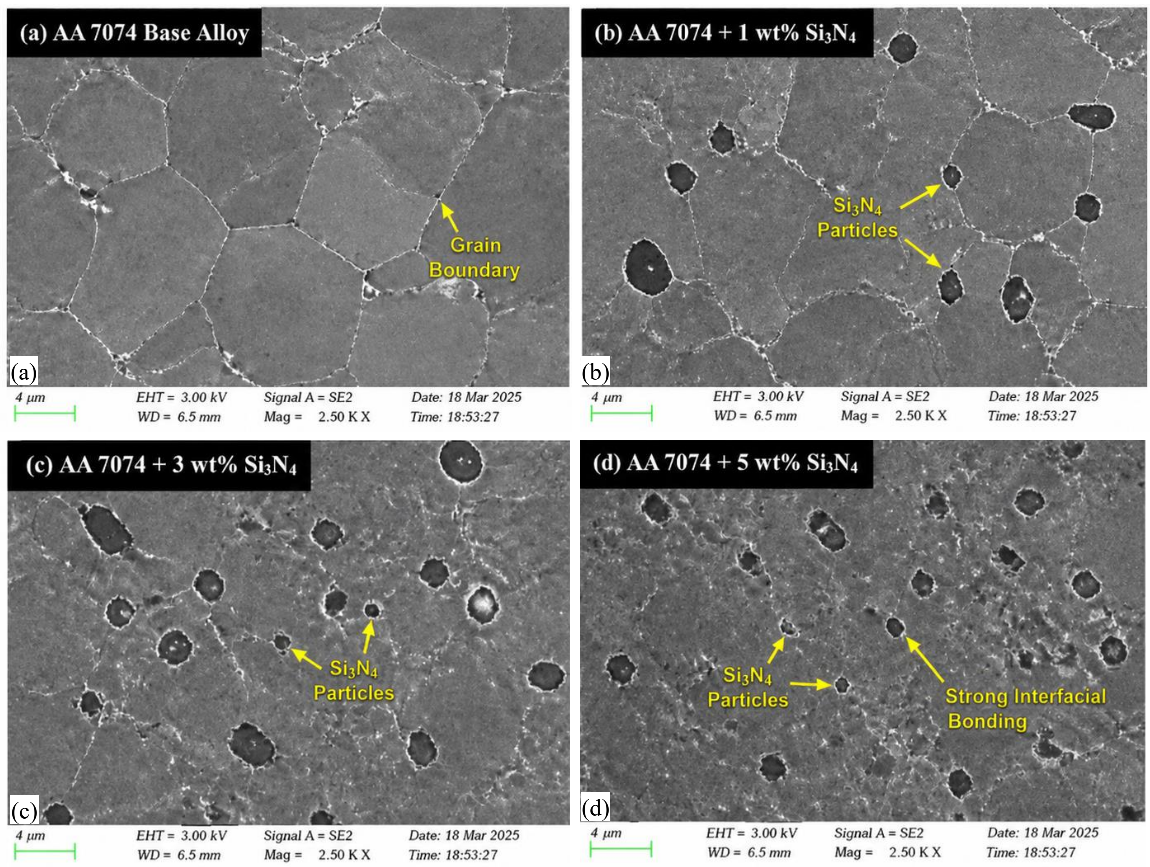

Figure 10. SEM images of (a) AA 7074 base alloy, (b) AA 7074 + 1 wt% Si_3N_4, (c) AA 7074 + 3 wt% Si_3N_4, and (d) AA 7074 + 5 wt% Si_3N_4 composites.

This indicates that the ceramic phase has begun to participate in strengthening, but the low reinforcement content provides only moderate improvement in load transfer and resistance to plastic deformation. The AA 7074 + 3 wt% Si_3N_4 composite shows better particle dispersion compared with the 1 wt% sample. The Si_3N_4 particles are more evenly distributed throughout the matrix, reducing localized particle-free regions. This improved dispersion supports better stress transfer from the softer aluminium matrix to the harder ceramic particles. It also restricts dislocation movement, which contributes to the observed increase in tensile strength, hardness, flexural strength, and impact resistance reported in the manuscript. The AA 7074 + 5 wt% Si_3N_4 composite exhibits the most uniform reinforcement distribution and stronger matrix–particle interfacial bonding. The ceramic particles appear well embedded in the AA 7074 matrix, suggesting effective incorporation during stir casting, extrusion, and heat treatment. This uniform structure reduces porosity, limits crack propagation, and improves resistance to localized deformation. The SEM observation supports the mechanical results, where the 5 wt% Si_3N_4 composite showed the best overall performance, including higher compressive strength, flexural strength, hardness, impact strength, and lower coefficient of friction. Overall, the SEM analysis confirms that increasing Si_3N_4 content improves the microstructural stability of AA 7074 composites. The transition from a plain aluminium matrix to a uniformly reinforced composite structure explains the enhancement in mechanical and tribological properties. The 5 wt% Si_3N_4 composite can therefore be considered the optimum composition, as it provides uniform particle dispersion, improved interfacial bonding, reduced crack initiation sites, and superior strengthening efficiency. Figure 10 shows the SEM images of (a) AA 7074 base alloy, (b) AA 7074 + 1 wt% Si_3N_4, (c) AA 7074 + 3 wt% Si_3N_4, and (d) AA 7074 + 5 wt% Si_3N_4 composites.

CONCLUSION

This study effectively manufactured AA 7074 aluminium alloy composites reinforced with silicon nitride (Si_3N_4) particles using stir casting, followed by extrusion and heat treatment. The main aim was to examine the influence of reinforcement content on the mechanical and tribological characteristics of the produced composites. The testing results exhibited a consistent enhancement in tensile, compressive, flexural, impact, and hardness parameters with the incorporation of Si_3N_4, as well as improved wear resistance. The 5 wt% reinforced composite had the highest tensile strength (109.84 MPa), flexural strength (29.65 MPa), and impact energy (17.6 J), concurrently exhibiting the lowest wear loss. Microstructural investigation verified a homogeneous distribution of ceramic particles inside the matrix, negligible porosity, and robust interfacial bonding, which combined enhanced the mechanical properties and fracture resistance. The comparison analysis confirmed that the reinforcement content significantly influenced the overall performance of the composites. The basic alloy had the lowest strength and hardness, but the reinforced samples, especially SN5, consistently excelled in all assessed characteristics. Si_3N_4 served as an efficient strengthening agent by refining grains, impeding dislocation movement, and hindering crack propagation. The advancements render the proposed AA 7074–Si_3N_4 composites viable options for structural, automotive, and aerospace applications necessitating lightweight materials with superior strength, durability, and wear resistance.

Declaration of Interest

The authors(s) have disclosed no conflicts of interest.

Acknowledgements

Not Applicable

Data Availability Statement

This study does not develop nor examines any new data

Ethics Statement

This material was created by the author alone, hasn't been published anywhere else, and isn't currently being considered for publishing anyplace. It fully and properly reflects the study and analysis of the author or authors.

Funding

Funding is not available to report.

REFERENCE

1. Kumar, G. V., Panigrahy, P. P., Nithika, S., & Rao, C. S. P. (2019). Assessment of mechanical and tribological characteristics of Silicon Nitride reinforced aluminum metal matrix composites. Composites Part B: Engineering, 175, 107138.
2. Kumaraswamy, J., Bharath, L., Anil, K. C., Geetha, T. M., & Nagesh, R. (2025). Results in mechanical properties and wear behaviour of AA6061-Si3N4 composites. Results in Surfaces and Interfaces, 18, 100376.
3. Ramesh, S., Gautam, S. K., Roy, H., Lohar, A. K., Samanta, S. K., Anand, A., ... & Kumar, S. (2024). Structure property correlation of gravity die-cast and rheocast Al–Mg–Sc–Zr in situ Nano-TiB2 composite. International Journal of Metalcasting, 18(4), 3095–3103.
4. Natrayan, & Navaneethakrishnan, B. (2024). Finger millet husk ash Si3N4 as an alternative mold material for green sand mold casting of AA7075 alloys: an optimization study. Biomass Conversion and Biorefinery, 14(23), 29689–29698.
5. Mohammed, M. M., Rasidi, M., Mohammed, A. M., Rahman, R. B., Osman, A. F., Adam, T., ... & Dahham, O. S. (2022). Interfacial bonding mechanisms of natural fibre-matrix composites: an overview. BioResources, 17(4), 7031.
6. Ashwin Prabhu, G., Selvam, R. & Kumar, K.M. Evaluating hybrid basalt and stainless-steel wire mesh laminated composites under low impact velocity tests for naval applications. J. Mater. Res. 40, 2169–2180 (2025).
7. Prasanth, G., Madhu, G. M., & Kottam, N. (2024). CeAlO3 nanoparticle synthesis through combustion-assisted method and structural property assessment in Nano-CeAlO3 polymer composites. Materials Technology, 39(1), 2330279.
8. Manawi, Y. M., Ihsanullah, Samara, A., Al-Ansari, T., & Atieh, M. A. (2018). A review of carbon nanomaterials’ synthesis via the chemical vapor deposition (CVD) method. Materials, 11(5), 822.
9. Kalidasan, B., Pandey, A. K., Saidur, R., Samykano, M., & Tyagi, V. V. (2023). Nano additive enhanced salt hydrate phase change materials for thermal energy storage. International Materials Reviews, 68(2), 140–183.
10. Stalin, B., Arivukkarasan, S., & Prabhu, G. A. (2015). Microstructure and mechanical properties evaluation of aluminium matrix reinforced with tungsten carbide and silicon carbide. International Journal of Applied Engineering Research, 10(55), 3994–3999.
11. Sun, F., Osenberg, M., Dong, K., Zhou, D., Hilger, A., Jafta, C. J., ... & Manke, I. (2018). Correlating morphological evolution of Li electrodes with degrading electrochemical performance of Li/LiCoO2 and Li/S battery systems: investigated by synchrotron X-ray phase contrast tomography. ACS Energy Letters, 3(2), 356–365.
12. Townsend, A., & Gouws, R. (2022). A comparative review of lead-acid, lithium-ion and ultra-capacitor technologies and their degradation mechanisms. Energies, 15(13), 4930.
13. Khalid, R., Shah, A., Javed, M., & Hussain, H. (2025). Progress and obstacles in electrode materials for lithium-ion batteries: a journey towards enhanced energy storage efficiency. RSC advances, 15(20), 15951–15998.
14. Hong, H., Mohamad, N. A. R. C., Chae, K., Mota, F. M., & Kim, D. H. (2021). The lithium metal anode in Li–S batteries: challenges and recent progress. Journal of Materials Chemistry A, 9(16), 10012–10038.
15. Pratheesh, K., Kaliappan, S., Natrayan, L., & Arthanarieswaran, V. P. (2024). Dry and wet sliding, fatigue, creep and mechanical properties of AA-7475 metal matrix composite reinforced with Si2N2O from rice husk ash. Journal of the Australian Ceramic Society, 1–12.
16. Prabhu, G.A., Selvam, R. & Kumar, K.M. (2024). Enhancing the Mechanical Properties of Basalt Fiber and Stainless Steel Wire Mesh Composites Incorporating Fire Retardants Through Response Surface Methodology Optimization. Fibers Polym 25, 1443–1455.
17. Yang, J. N., Xu, Y. X., Nie, S. B., Feng, X. S., & Jiang, L. (2021). Effect of organic-modified nickel phyllosilicates on the tribological, mechanical and thermal properties of epoxy composites. Journal of Materials Research and Technology, 14, 692–702.
18. Jayakanth, J., Chennakesavulu, K., Ramanjaneya Reddy, G., Dhanalakshmi, S., Priya, V., Sasikumar, K., & Sasipraba, T. (2023). A study on development of silicone rubber with conductive

carbon, polyaniline, MWCNT composite for EMI shielding. High performance polymers, 35(6), 547–558.
19. Gopal, V., Bharanidaran, R., Jesudass Thomas, S. et al. (2026). Design, fabrication and performance evaluation of a 3D-printed microgripper based on compliant mechanisms for precision manipulation. J Micro-Bio Robot 22, 1.
20. Aditya, I. D., Matsunaka, D., Shibutani, Y., & Yamamoto, G. (2017). First-principles study of interfacial interaction between carbon nanotube and Al2O3 (0001). Journal of Applied Physics, 121(2).
21. Kumeria, T., Santos, A., & Losic, D. (2014). Nanoporous anodic alumina platforms: engineered surface chemistry and structure for optical sensing applications. Sensors, 14(7), 11878–11918.
22. Natarajan, Eswara Prasath, Rasu, Karthick, Murugesan, Vigneshkumar and Gnanasekaran, Ashwin Prabhu. "Effect of basalt and kenaf fiber hybridization on the physical, mechanical, and thermal properties of polymer composites" Materials Testing, vol. 67, no. 11, 2025, pp. 1860–1869
23. Chizhov, A., Rumyantseva, M., & Gaskov, A. (2021). Light activation of nanocrystalline metal oxides for gas sensing: Principles, achievements, challenges. Nanomaterials, 11(4), 892.
24. Sun, F., Osenberg, M., Dong, K., Zhou, D., Hilger, A., Jafta, C. J., ... & Manke, I. (2018). Correlating morphological evolution of Li electrodes with degrading electrochemical performance of Li/LiCoO2 and Li/S battery systems: investigated by synchrotron X-ray phase contrast tomography. ACS Energy Letters, 3(2), 356–365.
25. Murali, M., Sambathkumar, M., & Saravanan, M. S. (2014). Micro structural and mechanical properties of AA 7075/TiO2 in situ composites. Universal Journal of Materials Science, 2(3), 49–53.
26. Rimikis, A., Kimmich, R., & Schneider, T. (2002). Investigation of n-values of composite superconductors. IEEE transactions on applied superconductivity, 10(1), 1239–1242.
27. Ashwin Prabhu, G., Selvam, R., Tiwari, V. et al. (2025). Optimizing hybrid composites: Enhancing mechanical properties with SiC and Al2O3 nanoparticles using response surface methodology. J. Mater. Res. 40, 2723–2734.
28. Hernández-Martínez, S. E., Cruz-Rivera, J. J., Garay-Reyes, C. G., & Hernández-Rivera, J. L. (2019). Experimental and numerical analyses of the consolidation process of AA 7075–2 wt.% ZrO2 powders by equal channel angular pressing. Journal of Materials Engineering and Performance, 28(1), 154–161.\
29. Masi, A., Armenio, A. A., Augieri, A., Celentano, G., Duchenko, A., Pompeo, N., ... & Varsano, F. (2024). Development of Ca/K-1144 IBS wires with composite Cu/Ta sheaths. IEEE Transactions on Applied Superconductivity, 34(3), 1–5.
30. Verma, P. K., Kaipamangalath, A., Varma, M. R., & Bai, V. S. (2023). Nonreactive Nano WO 3 Inclusions to Enhance Flux Pinning in Bi-2223 Superconductor Composites. IEEE Transactions on Applied Superconductivity, 34(1), 1–12.
31. Babu, N. H., Iida, K., Briffa, A., Shi, Y. H., Matthews, L. S., & Cardwell, D. A. (2007). Bulk superconducting nano-composites with high critical currents. IEEE transactions on applied superconductivity, 17(2), 2953–2956.
32. Nazareth, V. R., Sumption, M. D., Peng, X., Gregory, E., Tomsic, M. J., & Collings, E. W. (2008). Characterization of the A15 Layer Growth and Microstructure for Varying Heat Treatments in ${\rm Nb} _ {3}{\rm Sn} $ Tube Type Composites. IEEE transactions on applied superconductivity, 18(2), 1005–1009.
33. Kubit, A., Wydrzynski, D., & Trzepiecinski, T. (2018). Refill friction stir spot welding of 7075-T6 aluminium alloy single-lap joints with polymer sealant interlayer. Composite Structures, 201, 389–397.
34. Smoleń, J., Olesik, P., Stępień, K., Mikuśkiewicz, M., Myalska-Głowacka, H., Kozioł, M., ... & Godzierz, M. (2024). The influence of graphite filler on the self-lubricating properties of epoxy composites. Materials, 17(6), 1308.

35. Yu, T., Hu, C., & Li, Y. (2019). Functionalization of graphene and its influence on mechanical properties and flame retardancy of jute/poly (lactic acid) composite. Journal of Nanoscience and Nanotechnology, 19(11), 7074–7082.
36. Díaz, S., Romero, F., Suárez, L., Ríos, R., Alemán, M., Venuleo, M., & Ortega, Z. (2024). Characterization of microalgae biomass-based composites obtained through rotational molding. Polymers, 16(13), 1807.
37. Cooley, L. D., & Lee, P. J. (2002). Shift of the flux-pinning force curve in Nb/sub 3/Sn thin films with very fine grain size. IEEE transactions on applied superconductivity, 11(1), 3820–3823.
38. Sanivada, U. K., Mármol, G., Brito, F. P., & Fangueiro, R. (2020). PLA composites reinforced with flax and jute fibers—A review of recent trends, processing parameters and mechanical properties. Polymers, 12(10), 2373.
39. Gouda, P. S., Williams, J. D., Yasaee, M., Chatterjee, V., Jawali, D., Rahatekar, S. S., & Wisnom, M. R. (2016). Drawdown prepreg coating method using epoxy terminated butadiene nitrile rubber to improve fracture toughness of glass epoxy composites. Journal of Composite Materials, 50(7), 873–884.
40. Cure, B., Gaddi, A., Gerwig, H., Herve, A., & ten Kate, H. (2011). Conceptual Design of a 5 T, 6 m Long and 6 m Bore Solenoid for a Future Linear Collider Detector. IEEE transactions on applied superconductivity, 22(3), 4902304–4902304.

